Microchimica Acta (2019) 186: 46
https://doi.org/10.1007/s00604-018-3144-4

ORIGINAL PAPER

Amperometric sensing of hydrazine in environmental and biological samples by using CeO_2-encapsulated gold nanoparticles on reduced graphene oxide

Hong Huang[1] · Tingyu Li[2] · Yifan Sun[1] · Linghui Yu[2] · Changding Wang[1] · Rong Shen[2] · Weichun Ye[1] · Degui Wang[2] · Yumin Li[3]

Received: 27 October 2018 / Accepted: 2 December 2018 / Published online: 4 January 2019

Abstract

CeO_2-encapsulated gold nanoparticles (AuNPs) were anchored to reduced graphene oxide (RGO/Au@CeO_2) by an interfacial auto-redox reaction in a solution containing tetrachloroauric acid and Ce(III) on a solid support. The resulting material was placed on a glassy carbon electrode (GCE) and used as an electrochemical hydrazine sensor at trace levels. The electrocatalytic activity of the modified GCE towards hydrazine oxidation was significantly enhanced as compared to only RGO/CeO_2, or CeO_2-encapsulated AuNPs, or AuNPs loaded on CeO_2 modified with RGO. This enhancement is attributed to the excellent conductivity and large surface area of RGO, and the strong interaction between the reversible Ce^{4+}/Ce^{3+} and $Au^{\delta+}/Au^0$ redox systems. The kinetics of the hydrazine oxidation was studied by electrochemical methods. The sensor, best operated at a peak voltage of 0.35 V (vs. saturated calomel electrode), had a wide linear range (that extends from 10 nM to 3 mM), a low detection limit (3.0 nM), good selectivity and good stability. It was successfully employed for the monitoring of hydrazine in spiked environmental water samples and to in-vitro tracking of hydrazine in cells with respect to its potential cytotoxicity.

Keywords Encapsulation structure · Solid-solution interfacial autoredox reaction · Electrochemical sensor · In vitro cell detection

Introduction

Hydrazine has been extensitively used in fuel cells, rocket propellant, chemical reactions, industrial factories, corrosion inhibitors and photography chemicals [1]. Hydrazine is carcinogenic and mutagenic. Its long-term exposure can cause serious damage in brain, liver, lungs and kidneys [2]. According to the U.S. Environmental Protection Agency (EPA) regulations, the maximum hydrazine allowance level is as low as 10 ppb [3]. Therefore, it is highly desired for the development of an economical and convenient platform for sensitive detection of hydrazine. Compared with traditional methods reported for sensing hydrazine like chemiluminescence [4], chromatography [5] and fluorescence [6], electrochemical techniques are considered as the simple, sensitive and selective tools due to their fast response, easy of miniaturization, fast response, reproducibility and sensitivity.

Owing to the excellent electrical conductivity and high catalytic activity, gold nanoparticles (AuNPs) are one of the most interesting nanomaterials for the fabrication of novel chemical and biological sensors [7]. Many studies demonstrated that the decoration of noble metal NPs on the graphene or reduced graphene oxide (RGO) surface decreased their loading and significantly improved catalytic performance [8]. Furthermore, metal oxides are another important class of support materials for their relatively low cost and outstanding chemical stability. Especially, the synergic effect at the metal/metal oxide heterojunction is responsible for the enhanced catalytic performance which cannot be achieved with unsupported catalysts [9, 10]. As a key

Electronic supplementary material The online version of this article (https://doi.org/10.1007/s00604-018-3144-4) contains supplementary material, which is available to authorized users.

✉ Weichun Ye
yewch@lzu.edu.cn

✉ Degui Wang
wangdegui@lzu.edu.cn

✉ Yumin Li
liym@lzu.edu.cn

[1] State Key Laboratory of Applied Organic Chemistry and Department of Chemistry, Lanzhou University, Lanzhou 730000, China

[2] School of Basic Medical Sciences, Lanzhou, China, Lanzhou University, Lanzhou 730000, China

[3] Key Laboratory of Digestive System Tumors, Lanzhou University, Lanzhou 730000, China

component for many oxidation catalysts, CeO_2 with abundant oxygen vacancies is a typical of fluorite structure and shows excellent performance in catalysis. Also, CeO_2 has been particularly recognized as a very important support for metal nanoparticles in terms of its high oxygen storage capacity and the strong metal-support interaction effect [10]. For example, as dispersed Au atoms were supported on ceria, the interaction between the reversible Ce^{4+}/Ce^{3+} and $Au^{\delta+}/Au^0$ reductions ensured the high catalytic activity for CO oxidation. The amorphization of AuNPs on the CeO_x-RGO support yielded a high Faradaic efficiency in N_2 reduction under ambient conditions [11].

Chemical reduction is advantageous and favorable to the synthesis of AuNPs due to its versatility and simplicity. However, most strategies usually involve in the use of harsh reducing reagents such as sodium citrate, hydrazine, lithium (triethyl) borohydrate, and sodium borohydride [12]. Additionally, the form of simple surface loading greatly limits the metal-support interface and weakens the metal stability in harsh reaction conditions [13]. In order to solve the above problems, a solid-solution (S-S) interfacial autoredox reaction between noble metal ions in the precursor (solution) and Ce^{3+} in the support (solid) was proposed to fabricate CeO_2-encapsulated noble metals [10, 14, 15]. This synthesis method can obtain large scale core@shell nanostructures and avoid the sintering of noble metal NPs after heat treatment. Thus, the core@shell nanostructures exhibited effective inhibition of the migration in a long-term catalysis process. Nonetheless, this respect on the S-S interfacial autoredox reaction is still in the early stage and most involves in chemical catalysis. Consequently, the fabrication of clean and well-dispersed Au@CeO_2 as a chemical/biosensor by this method is still a challenge.

Inspired by the merits of the S-S interfacial autoredox reaction method, we employed this method to synthesize the RGO/Au@CeO_2 composite in this work, avoiding harsh reducing reagents. Due to the synergic effect of Au and CeO_2, the electrochemical sensor based on the materials presented excellent electroanalytical performance toward hydrazine oxidation, including wide linear rang, low limit of detection (LOD) and high selectivity. The sensor showed great promising for the detection of trace level hydrazine in environmental water samples such as tap, river and lake water as well as in biological systems.

Experimental section

Chemicals and materials

All reagents were of analytical grade and purchased from Sinopharm Chemical Reagent Co., China. $HAuCl_4$•$4H_2O$ and Hexadecyl trimethyl ammonium Bromide (CTAB) were supplied by Shanghai Macklin Biochemical. $Ce(NO_3)_3$•$6H_2O$ was purchased from Macklin Biochemical (www.macklin.cn). N_2H_4•H_2O was purchased from XiLong Chemical industry (www.xlhg.cn). GO was obtained from XF NANO Company (www.xfnano.com). Eagle's medium (DMEM, Hyclone) and Fetal Bovine Serum (FBS, PAN) (www.thermo.com) were produced commercially.

Characterization

Transmission electron microscopy (TEM) and selected area electron diffraction (SAED) were characterized with a Tecnai G2 F30 (FEI, USA). X-ray powder diffraction (XRD) analysis was carried out on Rigaku D/max-2400 (Cu K-Alpha radiation, $\lambda = 0.1541$ nm). X-ray photoelectron spectroscopy (XPS) was acquired by a multifunctional spectrometer (Thermo Scientific) using Al Radiation. Raman spectra were obtained with a confocal Raman spectrography (Zolix Finder Vista-HiR; laser excitation at 532 nm with a power of 4 mW). UV-vis absorption spectra were recorded using a UV-2102C Model spectrometer.

Electrochemical experiments were carried out on an electrochemical work station (CHI660B, Shanghai China) with a three-electrode system. The counter and reference electrodes were a platinum wire and saturated calomel electrode (SCE), respectively. The conditions were optimized and a glassy carbon electrode (3 mm diameter) as a working electrode was modified with 4, 6 and 8 μl of electrocatalyst ink (1 mg mL^{-1}), and 6 μL was taken for subsequent experiments. The electrolyte was 10 mL phosphate buffered saline (PBS) (0.1 M, pH 7.5), except when mentioned.

Synthesis of RGO/Au@CeO_2 composite

10 mg of GO was firstly dispersed in 50 mL H_2O via a sonication. 290 μL $HAuCl_4$ (0.02 g mL^{-1}) and 1.4 mL $Ce(NO_3)_3$ aqueous solution (0.1 M) were added into the GO colloid solution at 5 °C (ice bath) under stirring. Then, 3 mL of ammonia solution (28 wt%) was rapidly added into the mixture solution. After stirring for 30 s, 3 mL of $Ce(NO_3)_3$ aqueous solution (0.047 M) was rapidly injected and kept for 20 min. The product was collected by centrifugation, washed with water and ethanol, and dried in vacuum in sequence. Finally, the RGO/Au@CeO_2 product was annealed to 300 °C under N_2 atmosphere for 6 h with a heating rate of 2 °C min^{-1}.

The preparation of Au@CeO_2 and RGO/CeO_2 was performed under the same conditions without the precursor of GO or $HAuCl_4$.

As a comparison, the surface-loading AuNPs on RGO/CeO_2 (RGO/CeO_2-$Au_{(s)}$) were prepared by chemical reduction. Typically, the RGO/CeO_2 was dispersed in water, and a proper amount of $HAuCl_4$ solution was added to the mixture dropwise with stirred. Subsequently, 1 mL of $NaBH_4$ solution (0.1 M) was added slowly. After being collected by centrifugation, washed with water and ethanol, the RGO/CeO_2-$Au_{(s)}$

product was annealed to 300 °C under N_2 atmosphere for 6 h with a heating rate of 2 °C min^{-1}.

Cell cytotoxicity assay and determination of N_2H_4 incubated in HEK-293 cells

HEK-293 cells (Human embryonic kidney cells 293) were cultured in Dulbecco's modified Eagle's medium (DMEM, Hyclone, USA) containing 10% Feral Bovine Serum (FBS, PAN, Germany) in an incubator containing 5% CO_2 at 37 °C. The cell viability assay was determined by CCK-8 kit according to the manufacturer's protocols: In brief, HEK-293 cells (10^4 cells/well) were seeded into 96-well plates for 24 h. Then, different concentrations of RGO/Au@CeO_2 and RGO/CeO_2-$Au_{(s)}$ solution were added and incubated for 12 and 24 h, respectively. Finally, the CCK-8 reagent was added into each well and treated for 3 h. The absorbance at 450 nm was measured by a microplate reader (Bio-Tek, Winooski, VT, USA).

HEK-293 cells (10^5 cells/well) were seeded into 6-well plates for 24 h. 80 μM N_2H_4 aqueous solution was added into each well for 12 and 24 h cultivation, respectively. Then, the cells were collected and washed for twice by 0.1 M PBS. After that, the cells were broken using the freezing and thawing technique for three times. Based on the three-electrode system, an amperometric response at 0.35 V (vs. SCE) was recorded to detect the hydrazine content in the collected cell samples.

Results and discussion

Physical characterization

It has been reported that Ce^{3+} exhibits reducing capability in alkaline conditions [16]. A redox reaction can be easily triggered on the S–S interface between $AuCl_4^-$ and Ce^{3+}, which can be expressed by Eq. (1):

$$AuC1_{4^-} + 3Ce^{3+} = Au + 3Ce^{4+} + 4C1^- \quad (1)$$

Obviously, the redox reaction is responsible for the formation of AuNPs and CeO_2 upon the addition of ammonia solution. The colour of the mixture changes from almost colourless to light grey at the beginning and then to purple, which proves the formation of AuNPs [17]. The formation of the RGO/Au@CeO_2 composite was confirmed by TEM. The low-magnification TEM image in Fig. 1a displays the core@shell structure of Au@CeO_2. AuNPs with an average size of 10 nm are tightly coated by CeO_2 NPs, where CeO_2 NPs are supported on the surface of RGO. In the HRTEM image (Fig. 1b), the interplanar spacing of 0.316 nm is assigned to the (111) facet of CeO_2 [14]; the the lattice fringe with 0.236 nm corresponds to Au (111). Similarly, two sets of diffracted spots in the SAED pattern (Fig. 1c) are in accord with the Au and CeO_2 phases. The EDX spectrum (Fig. 1d) reveals that the X-ray peaks of C, Au, Ce, and O match with the element analysis of RGO/Au@CeO_2 composite, except the element of Cu from the copper mesh.

The crystalline structure of RGO/Au@CeO_2 composite was characterized with Raman and XRD. In Raman spectrum (Fig. 1e), two characteristic peaks at 1348 and 1595 cm^{-1} are indexed to the D and G bands of graphene, respectively. And a sharp peak at 453 cm^{-1} is associated with the CeO_2 crystalline [18]. From the XRD pattern (Fig. 1f), all peaks are well indexed to the fluorite structure of CeO_2 (JCPDS No. 34–03494) and face-centered cubic (*fcc*) Au (JCPDS No. 001–1172). A weak diffraction peak appears at 23.6 ° due to the small amount of graphene, which indicates that GO is converted to RGO as the conjugated graphene network [19]. Moreover, no impurities are discernible.

For comparison, we added the strong reducing agent ($NaBH_4$) into the reaction system. Distinctly, $HAuCl_4$ was firstly reduced by $NaBH_4$, which led to the loading of AuNPs on the surface of CeO_2 NPs. The phenomenon was proved by the TEM image (Fig. S1). We compared the UV-vis absorption spectra of RGO/Au@CeO_2 and RGO/CeO_2-Au(s), as shown in Fig. S2. The surface plasmon resonance (SPR) peak of AuNPs for the surface loading locates at 546 nm. However, as AuNPs are embedded into CeO_2 NPs, the peak occurs a red-shift at 559 nm. This also proves the formation of CeO_2-encapsulated AuNPs from the S-S interfacial autoredox reaction [20]. Additionally, Au@CeO_2 and RGO/CeO_2 were prepared by the same method without adding the GO or $HAuCl_4$ precursor. Their structure and composition were confirmed by the Raman spectra and XRD patterns, as shown in Fig. S3.

Electrochemical oxidation of hydrazine

We studied the electrochemical behaviors of our newly synthesized catalysts for electrochemical oxidation of hydrazine in 0.1 M PBS (pH 7.5). The inset of Fig. 2a shows the cyclic voltammograms (CVs) over RGO/Au@CeO_2 in the presence (plot a) and absence (plot b) of 3 mM hydrazine in the potential scanning from −0.6 to 0.8 V. No oxidation peaks are observed in hydrazine-free solution, whereas an oxidation peak appears at 0.35 V on adding hydrazine. This can be assigned to the oxidation of hydrazine to nitrogen in the potential range [21]. We further compared its electrocatalytic activity with RGO/CeO_2-$Au_{(s)}$, Au@CeO_2 and RGO/CeO_2 by using cyclic voltammetry, as shown in Fig. 2a and Table S1. Similarly, no oxidation peaks are observed for pure RGO/CeO_2. However, as AuNPs are modified on the RGO/CeO_2 or CeO_2, the peak toward hydrazine oxidation is observed at about 0.35 V. The peak current of RGO/Au@CeO_2 is 563.2 μA. However, as using the surface loading method, the prepared catalyst (RGO/CeO_2-Au(s)) only exhibits the peak current of 450.1 μA.

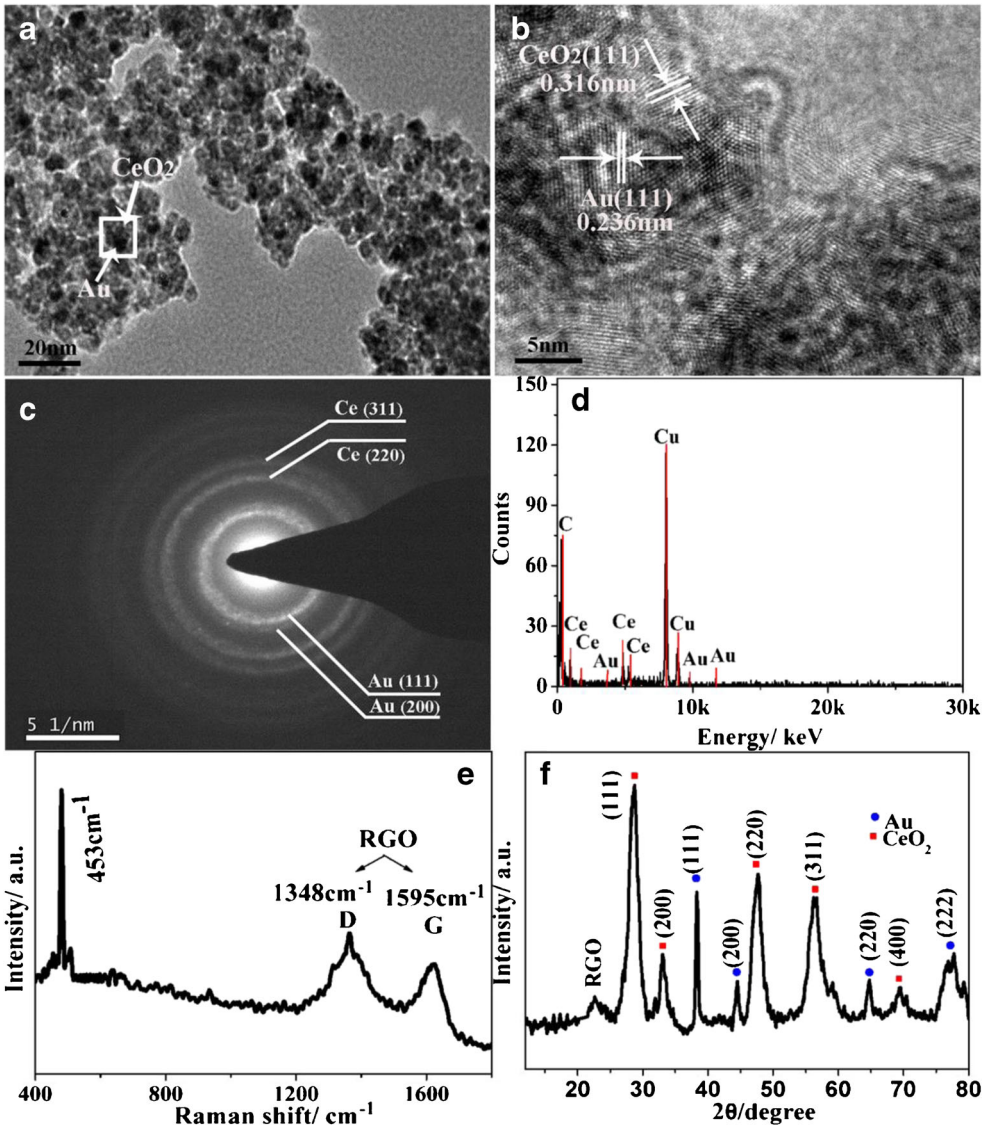

Fig. 1 Morphology and structure characterization of the RGO/Au@CeO_2 composite: TEM (**a**) and HRTEM (**b**) images; SAED (**c**), EDX (**d**) and Raman (**e**) spectra; XRD pattern (**f**)

Additionally, the excellent conductivity of RGO is also another factor. For Au@CeO_2, its peak current is just 308.3 μA.

Tafel plot is another common electrochemical method to test the electrocatalytic performance. Similarly, RGO/Au@CeO_2 presents the lowest Tafel slope among these catalysts (Fig. 2b and Table S1). The lower Tafel slope means the higher catalytic activity [22]. Therefore, the parameters from Tafel plots prove that RGO/CeO_2@Au possesses superior catalytic activity. The behavior of electron transfer between the electrolyte and the catalyst was studied by using $[Fe(CN)_6]^{4-/3-}$ as the electrochemical probe. Figure 2c shows the Nyquist plots over the above catalysts. This experimental design can be described regarding a simple electrical equivalent circuit as illustrated in Fig. S4. In Table S2, the corresponding parameters for the equivalent circuit model are obtained. Here, the electron transfer resistance, R_{ct}, is usually used to evaluate electron transfer rate [23]. Obviously, the R_{ct} value of RGO/Au@CeO_2 is the lowest among these materials. These demonstrate that RGO/Au@CeO_2 can facilitate the enhanced electrocatalytic activity due to the efficient electron transfer. Furthermore, the electrocatalytic stability is an important factor for an electrocatalyst. Figure 2d shows the chronoamperograms of the catalysts at 0.35 V for hydrazine oxidation. The steady-state current (*I*) of RGO/Au@CeO_2 is the highest during the whole testing time.

The satisfied electrocatalytic performance of RGO/Au@CeO_2 was studied by XPS analyzing its chemical states. The detailed analysis is shown in the ESM. Briefly, In Fig. S5, C, O, Ce, and Au elements can be distinctly seen. And the Ce 3d peaks can be fitted to Ce^{3+} and Ce^{4+} peaks, which suggests that the catalyst holds both Ce^{3+} and Ce^{4+} ions after the calcination [24]. For Au 4f, the binding energy (BE) peaks at 83.8 and 87.5 eV are attributed to the Au $4f_{7/2}$ and Au $4f_{5/2}$ spin-orbits (respectively), which are the characteristic peaks of Au^0. Their BEs occur positive shift by 0.3 eV as compared with pure metallic Au^0. These indicate a down-shift of d-band centre of Au with respect to the Fermi level [25]. So, the co-

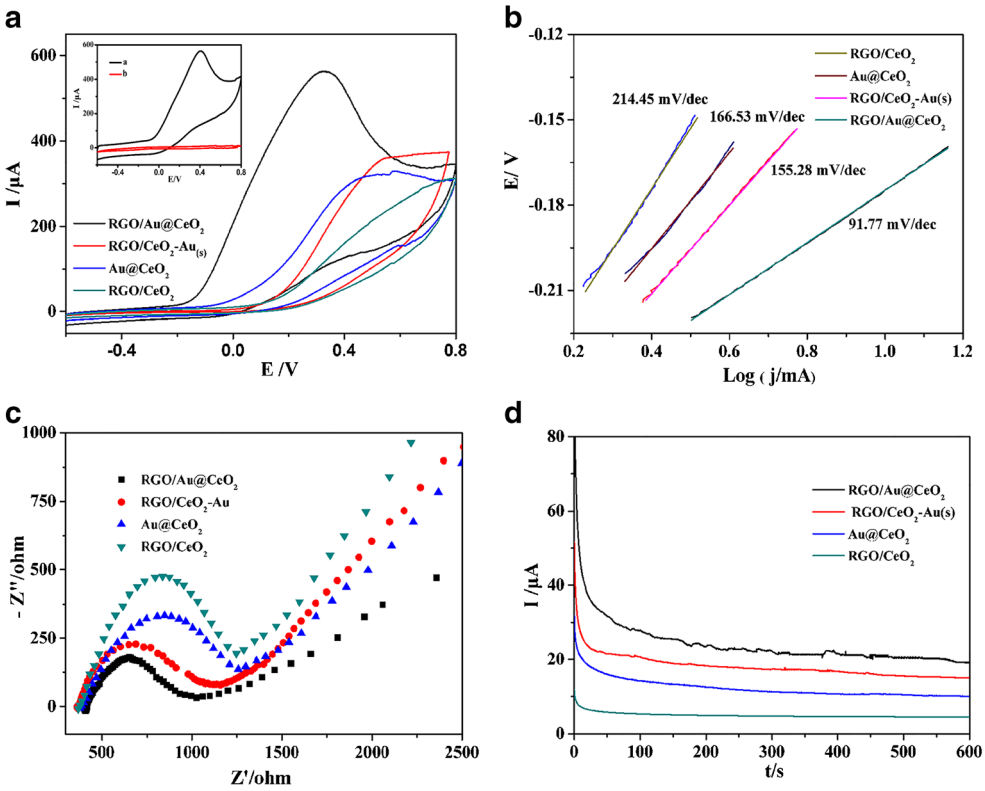

Fig. 2 Comparison of the electrochemical behaviors: CVs at a scan rate of 100 mV s^{-1} (**a**), Tafel plots (**b**), EIS plots (**c**) and chronoamperograms at 0.35 V (**d**) over RGO/Au@CeO_2, RGO/CeO_2-$Au_{(s)}$, Au@CeO_2 and RGO/CeO_2. In (**a**), (**b**) and (**d**), the electrolyte was 0.1 M PBS (pH 7.5) containing 3 mM hydrazine. In (**c**), the electrolyte was 0.1 M KCl containing 5 mM $[Fe(CN)_6]^{4-/3-}$. The inset of (**a**) shows the CVs over RGO/Au@CeO_2 in 0.1 M PBS (pH 7.5) with (a) or without (b) 3 mM hydrazine

existence of Au^0 and $Au^{\delta+}$ species in RGO/Au@CeO_2 can effectively accelerate the catalytic efficiency owing to the strong interaction between the reversible Ce^{4+}/ Ce^{3+} and $Au^{\delta+}/Au^0$ reductions (Scheme 1).

Kinetic study of hydrazine oxidation

The study of the scan rate effect may provide the kinetic information of hydrazine oxidation. A series of CVs of RGO/Au@CeO_2 are shown in Fig. 3a in 0.1 M PBS (pH 7.5) containing 3.0 mM hydrazine at different scan rates (40 to 200 mV s^{-1}). It is found that the oxidation peak current increases with the increase of scan rate, in company with the positive shift of the peak potential. Interestingly, the oxidation peak current displays a linear relationship with the square root of scan rate (Fig. 3b), indicating that the oxidation of hydrazine may be a diffusion controlled process. It is well-documented that the electrochemical oxidation of hydrazine involves in a 4-electron process [2]. The outstanding electrochemical response process of hydrazine oxidation over RGO/Au@CeO_2 can be explained by kinetic adsorption of hydrazine on the electrode surface and the following electrochemical oxidation, as displayed in Scheme 1.

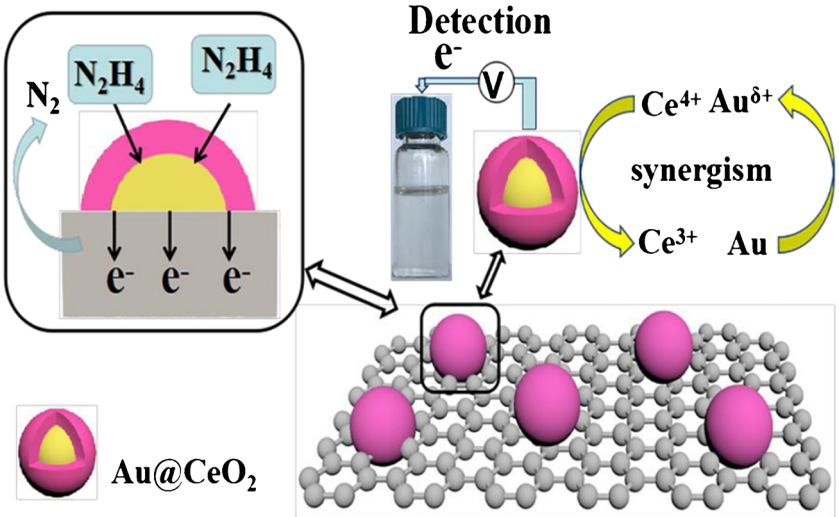

Scheme 1 Schematic illustration of the electrochemical response of RGO/Au@CeO_2 to hydrazine oxidation

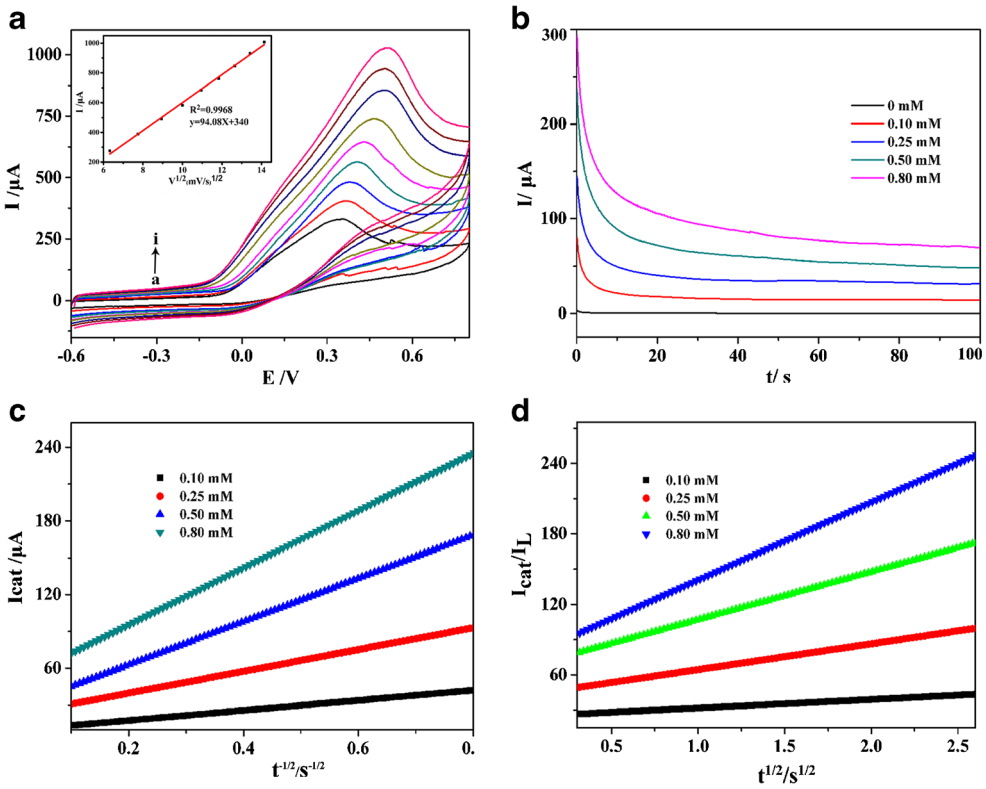

Fig. 3 Electrochemical sensing hydrazine over RGO/Au@CeO_2: **a** CVs at different scan rates (from a to i: 40, 60, 80, 100, 120, 140, 160, 180, 200 mV s^{-1}) in 0.1 M PBS (pH 7.5) containing 3 mM hydrazine; **b** Chronoamperometric responses with various concentrations (from 0 to 0.80 mM) of hydrazine; **c** The plot of I_{cat} vs $t^{-1/2}$; **d** The plot of I_{cat}/I_L vs $t^{1/2}$. The inset of (**a**) show the $v^{1/2}$ vs I_p plot

Figure 3b shows the chronoamperometric response of RGO/Au@CeO_2 in the absence and presence of various concentrations (from 0.10 to 0.80 mM) of hydrazine. It is observed that the steady currents improve with the hydrazine concentration. Herein, the catalytic rate constant (K_{cat}) can be estimated according to Eq. (2) [26]:

$$I_{cat}/I_L = (\pi K_{cat} C_0 t)^{1/2} \quad (2)$$

where I_{cat} and I_L are the currents of RGO/Au@CeO_2 in presence and absence of hydrazine, respectively. From the slopes of the linear plots of I_{cat}/I_L versus $t^{1/2}$ (Fig. 3c), the average value of K_{cat} can be calculated to be 7.13×10^3 M^{-1} s^{-1}. The value is larger than the previously reported values based on benzothiazole-iron oxide nanoparticles modified carbon paste electrode (5.1×10^3 M^{-1} s^{-1}) [27] and cobalt pentacyanonitrosyl ferrate (2.2×10^3 M^{-1} s^{-1}) [28]. So, it is believed that RGO/Au@CeO_2 has an excellent electrocatalytic activity toward hydrazine oxidation.

In addition, the diffusion coefficient (D) of hydrazine in the system is determined by Eq. (3) [26]:

$$I_{cat} = nFAD^{1/2} C_0 \pi^{-1/2} t^{-1/2} \quad (3)$$

where A the electrode area, the other symbols are the same with the aforementioned equations. We can obtain the linear plots of I_{cat} versus $t^{-1/2}$ (Fig. 3d). The calculated value of D is 8.67×10^{-6} cm^{-1} s^{-1} from their slopes, which is very close to the previous report [21].

Electrochemical sensing of hydrazine

We firstly optimized the detection conditions like the solution pH and applied potential. The detailed results are shown in the ESM and Fig. S6. In this work, the optimized pH and applied potential were selected as 7.5 and 0.35 V (vs. SCE) (respectively) for the following measurements.

Figure 4a displays the *i-t* plot of the RGO/Au@CeO_2 modified GCE with successive injection of hydrazine into 0.1 M PBS (pH 7.5) at 0.35 V. Upon each injection of hydrazine, a well stair-shaped amperometric response is raised quickly. This response time of less than 3 s indicates the fast electrooxidation of hydrazine over this electrode. It is found that the response currents are linear with the concentration of hydrazine. The corresponding calibration plot for the RGO/Au@CeO_2 modified GCE are shown in Fig. 4b, c. Here, the relationship includes two linear slopes: one is in the range of 0.01 to 30 μM ($R^2 = 0.9976$) and the other ranges from 30 to 3000 μM ($R^2 = 0.9982$). According to the linear slopes, the sensitivities of the RGO/Au@CeO_2 modified electrode are calculated to be 25.62 μA mM^{-1} cm^{-2} (0.01–30 μM) and 1.70 μA mM^{-1} cm^{-2} (30–3000 μM). The great difference of the sensitivities between the low concentration and the high concentration can be attributed to the different oxidation kinetic process of hydrazine at different concentrations: In the low concentration region of hydrazine, the adsorption of hydrazine on the sensing interface is the

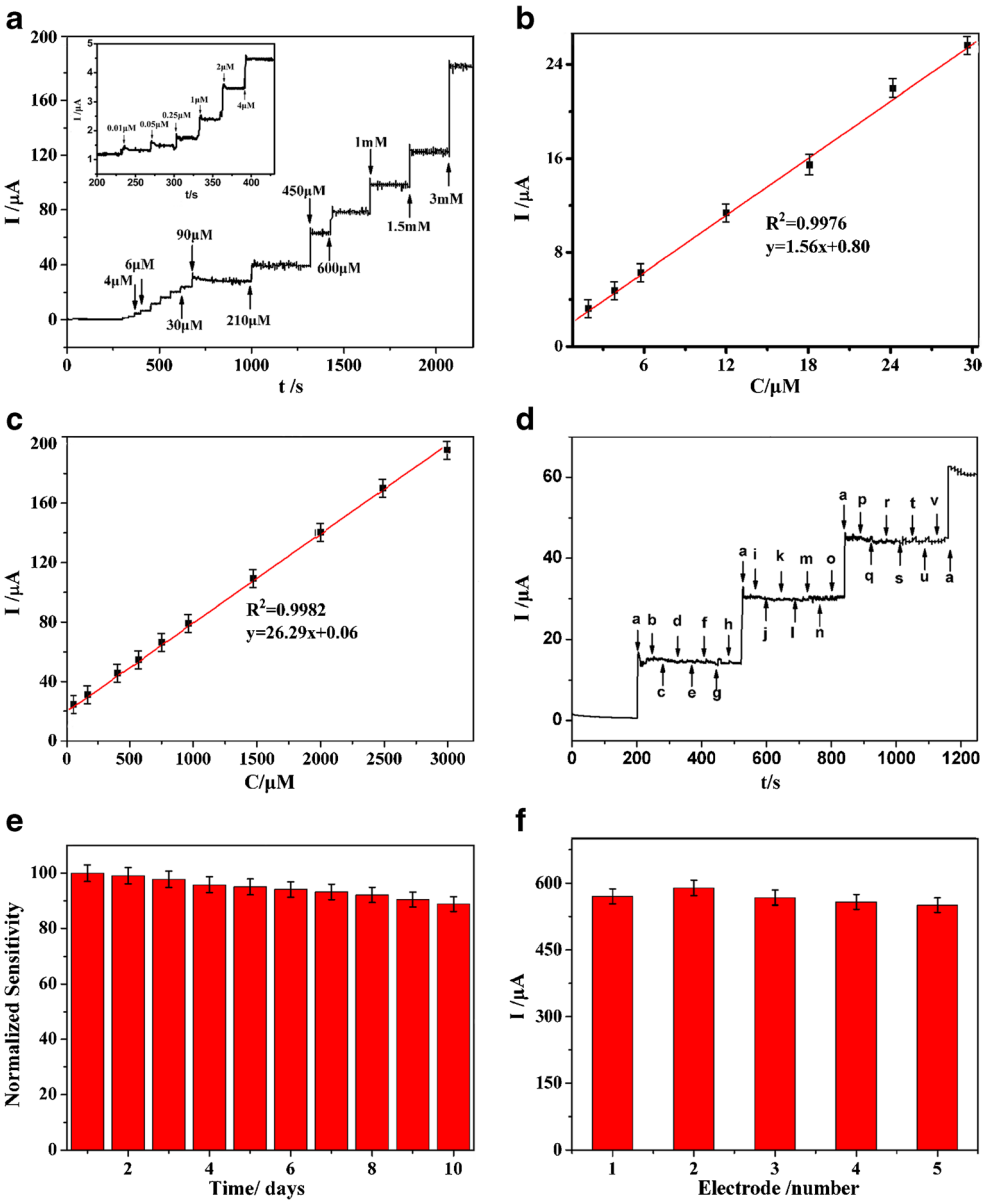

Fig. 4 **a** Amperometric responses of RGO/Au@CeO_2 to successive addition of hydrazine into 0.1 M PBS (pH 7.5) under stirring at applied potential of 0.35 V. Calibration plots in the range of 0.01–30 μM (**b**) and 30–3000 μM (**c**). (**d**) Amperometric response of RGO/Au@CeO_2 for 0.1 mM hydrazine (a) in presence of 300-fold quantities of $FeSO_4$ (b), NH_4Cl (c), $NiSO_4$ (d), KCl (e), NaCl (g), $CaCl_2$ (h), $MgSO_4$ (i),$CuSO_4$ (j),$CoCl_2$ (k), Zn $(NO_3)_2$ (l) and $MnSO_4$ (m), and 500-fold organic compounds like urea (f) lactose(n), glucose (o), ascorbic acid (p), 4-nitrophenol (q), quinol (r), ethylenediamine (s), tea polyphenol (t), adenine (u) and L-cystine (v) in the continuously 0.1 M PBS under stirring at the applied potential of 0.35 V. (E) Test stability of RGO/Au@CeO_2 in hydrazine solution during 10 days for each day test. (F) Comparison of electrochemical behaviors of RGO/Au@CeO_2 modified with five different GCEs: the scan rate was 100 mV s^{-1}. Error bars in the (E) and (F) represent the standard deviations of five times for each measurement

dominated controlling step with a high sensitivity; whereas, in the high concentration, the electrocatalytic activation of hydrazine on the electrode surface becomes the rate-determining step, and thus holding a decreased sensitivity [29].

The LOD can be estimated through the formula: LOD = $3S_d/b$, where S_d is the standard deviation of blank signal and b is the slope of the calibration plot. The LOD of our sensor is only 3.0 nM. This comparison represents that the RGO/Au@CeO_2-modified sensor has a reasonable performance for hydrazine sensing with relatively wider linear range and lower LOD, as compared to a variety of nanomaterials reported in literatures [30–34] (Table 1), In spite of an inferior LOD than TiO_2 film [9] and Au/NH_2MIL-125(Ti) [15], the higher sensitivity of our sensor is achieved. Also, the sensing material of RGO/Au@CeO_2 used in this work is environmental-friendly and ease for preparation.

In addition, a good selectivity is important for the utilization of an electrochemical sensor. In this work, the effects of various interfering species on the electrocatalytic activity toward hydrazine oxidation were checked under the optimized conditions. Figure 4d shows the amperometric responses to these interfering specie. As 300-fold common inorganic ions such as K^+, Na^+, Ni^{2+}, Ca^{2+}, Zn^{2+},Cu^{2+}, Fe^{2+}, Mg^{2+}, Mn^{2+}, NH_4^+, Co^{2+}, Cl^-, NO_3^-, CO_3^{2-} and SO_4^{2-}, and 500-fold organic compounds like urea, lactose, glucose (G), ascorbic acid (AA), 4-nitrophenol (4-NP), quinol, ethylenediamine, tea polyphenol, adenine and L-cystine are introduced, as we expect, there is no significant amperometric response in this sensor. Contrarily, when 0.1 mM hydrazine is injected into the electrolyte, obvious steps are observed. The results confirm that the RGO/Au@CeO_2 is a proper electrode material for hydrazine detection without explicit interference of numerous inorganic and organic species.

Table 1 Comparison of analytical parameters for the determination of hydrazine at RGO/Au@CeO_2 with other previously reported hydrazine sensors

Material	Method	Linear range (μM)	LOD (nM)	Sensitivity ($\mu A \cdot \mu M^{-1} \cdot cm^{-2}$)	Refs.
TiO_2 NPs	i-v	0.001–10,000	0.0288	35.04	[9]
Au/NH_2MIL-125(Ti)	amperometric	0.01–10	0.5	/	[15]
AuNP-MWCNT	amperometric	0.1–1000	3	4.98	[30]
PB/Fe_3O_4@rGO	amperometric	0.12–9	13.7	97.73	[31]
Fe_3O_4/PPy/GO	amperometric	5–1275	1400	449.7	[32]
Tungstophosphate-PAni/silver NCs	i-v	0.01–10,000	2.8	12.5	[33]
Fe_2O_3/CeO_2 NCs	amperometric	0.02–20,000	7.4	0.1275	[34]
Au-CeO_2/RGO	amperometric	0.01–30 30–3000	3	2208.06 12.40	This work

The stability of this sensor was further tested. Before being tested, the electrode was stored in ambient environments. The electrochemical response was successively measured in the presence of 0.1 mM hydrazine by cyclic voltammetry on the same electrode every day within ten days. From Fig. 4e, the catalytic current still maintains over 90% of the initial amperometric response after ten days. Similarly, good reproductivity with the relative standard deviation (RSD) of 3% is achieved when five different GCE electrodes modified with RGO/Au@CeO_2 have been employed according to the reproducibility assays (Fig. 4f). In term of the error bar data, the RSD values are determined to be within 5% for five measurements of one modified electrode. These tests demonstrate good repeatability of this electrochemical sensor.

Application to real samples

Determination of hydrazine in environmental water samples

Based on the above excellent properties such as high sensitivity, good selectivity, stability, reproductivity and repeatability, this electrochemical sensor was explored for determining trace level hydrazine in environmental water samples including tap water, Yellow River water and local lake water. These analyses were performed for three times under the same conditions by the standard addition method. The results are summarized in Table S3. The recoveries for hydrazine detection range from 99.2% to 100.9% and the RSD values are limited in 2.7%. The satisfactory recoveries and RSD values indicate that this electrochemical sensor is suitable for hydrazine detection in various environmental water samples.

Cytotoxicity test and in vitro tracking of hydrazine incubated into cells

Owing to the high performance of the electrochemical sensing platform in aqueous solution, the feasibility of hydrazine sensing was further demonstrated in cell samples. The cytotoxicity of the material in HEK-293 cells was firstly tested. From the MTT assay, the cells remain high cell survival rate upon treatment with 0.0–100.0 μg mL^{-1} RGO/Au@CeO_2 for 24 h (Fig. 5a). Even as its concentration is 100.0 μg mL^{-1}, the cell

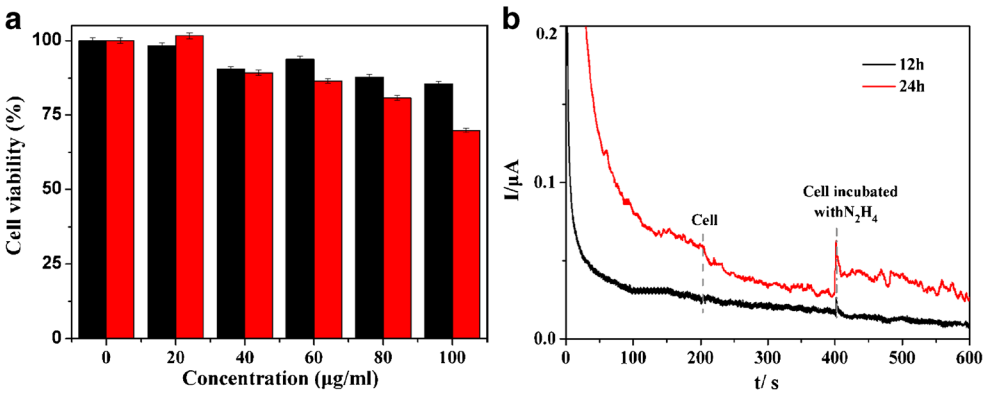

Fig. 5 **a** MTT assay of RGO/Au@CeO_2 (black) and RGO/CeO_2–$Au_{(s)}$ (red) with HEK-293 cells. HEK-293 cells were incubated with different concentration of RGO/Au@CeO_2 and RGO/CeO_2–$Au_{(s)}$ for 24 h, and cell viability was estimated through standard MTT assay. Error bars represent the standard deviations of three times for each measurement. **b** Amperometric responses of the electrode to the addition of the broken HEK-293 cell samples and cells incubated with hydrazine for 12 and 24 h, respectively. The applied potential was conducted at 0.35 V

survival rate always keeps over 85%. By contrast, for 100.0 μg mL^{-1} of RGO/CeO_2-$Au_{(s)}$, the cell survival rate is only 70% under the same conditions. The MTT assay indicates that RGO/Au@CeO_2 has low cytotoxicity to the cultured cells, which is benefited from the unique encapsulation structure.

We carried out the in vitro experiment to track the content of hydrazine in cell samples, where hydrazine was first incubated into HEK-293 cells and the cells were dispersed in 10 mL PBS solution for the electrochemical measurement after being washed with PBS solution and broken. The electrochemical results are illustrated in Fig. 5b. For 12 h incubation with hydrazine, a sensitive response in current is observed. With larger incubation time (24 h), the current increases significantly, presenting the maximum current change of about 0.07 μA. In comparison, no distinct current response is observed after the addition of HEK-293 cells without hydrazine incubation. In spite of the limits of our conditions, we believe that the material of RGO/Au@CeO_2 will hold great potential for biological applications including in vivo and in vitro evaluation by means of its low cytotoxicity and excellent electrochemical activity and specificity toward hydrazine oxidation. According to the above analysis, our established electrochemical sensor based on the novel material has the advantages of rapid and sensitive detection of hydrazine in the environmental and biological samples. However, electrochemical methods are still subject to matrix interference especially in complex water and in vivo biological matrix. To overcome this defectiveness, deepen experiments need to be performed to improve the related stability of the method.

Conclusions

We have successfully synthesized the RGO/Au@CeO_2 composite with an encapsulation structure through a S-S interfacial redox reaction, where no any harsh reducing agents were introduced. The composite was systematically characterized by XRD, SEM, TEM and XPS. Due to the synergic effect of Au and CeO_2 which was verified by XPS, the RGO/Au@CeO_2 composite exhibited outstanding electrocatalytic activity of hydrazine oxidation. This composite was further employed to fabricate an electrochemical sensor for sensitive and selective determination of hydrazine. A high-performance amperometric response, low LOD, wide linear range, good selectivity, stability and reproductivity were achieved. Interestingly, this electrochemical sensor was successfully used to detect trace level hydrazine in real river water, tap water and lake water, and also to in vitro track hydrazine in cell samples. It is expected that the environmental-friendly preparation strategy and high reliability of RGO/Au@CeO_2 can be developed to be a potential candidate for other sensor applications in various environmental and biological systems.

Acknowledgements This work is supported by the Fundamental Research Fund for the Central Universities (Nos. lzujbky-2017-k9) and the Natural Science Foundation of Gansu Province, China (No. 17JR5RA209).

Compliance with ethical standards The author(s) declare that they have no competing interests.

References

1. Amiripour F, Azizi SN, Ghasemi S (2018) Gold-copper bimetallic nanoparticles supported on nano P zeolite modified carbon paste electrode as an efficient electrocatalyst and sensitive sensor for determination of hydrazine. Biosens Bioelectron 30:111–117
2. Ju ZY, Li DP, Zhang D, Li DD, Wu CZ, Xu ZH (2017) An ESIPT-based fluorescent probe for hydrazine detection in aqueous solution and its application in living cells. Microchim Acta 27:679–687
3. Environmental Protection Agency (EPA) (1999) Integrated risk information system (IRIS) on hydrazine/hydrazine sulfate, in: national center for environmental assessment, office of research and development. Washington DC
4. Iranifam M (2016) Chemiluminescence reactions enhanced by silver nanoparticles and silver alloy nanoparticles: applications in analytical chemistry. Anal Chem 82:126–142
5. Han Q, Aydan T, Yang L, Zhang X, Liang Q, Ding M (2018) In-syringe solid-phase extraction for on-site sampling of pyrethroids in environmental water samples. Anal Chim Acta 1009:48–55
6. Lu Z, Shi X, Ma Y, Fan W, Lu Y, Wang Z (2018) A simple two-output near-infrared fluorescent probe for hydrazinedetection in living cells and mice. Sensors Actuators B Chem 258:42–49
7. Chen Y, Xian YY, Jiang X (2017) Surface modification of gold nanoparticles with small molecules for biochemical analysis. Acc Chem Res 50:310–319
8. Yao TH, Guo X, Qin S-C, Xia FY, Li YL, Chen Q, Li JS, He DY (2017) Effect of RGO coating on interconnected Co_3O_4 nanosheets and improved supercapacitive behavior of Co_3O_4/rGO/NF architecture. Nano-Micro Lett. 9:38
9. Rahman MM, Alfonso VG, Fabregat-Santiago F, Bisquert J, Asiri AM, Alshehri AA, Albar HA (2017) Hydrazine sensors development based on a glassy carbon electrode modified with a nanostructured TiO_2 films by electrochemical approach. Microchim Acta 184:2123–2129
10. Du JS, Bian T, Yu J, Jiang Y, Wang X, Yan Y, Jiang Y, Jin C, Zhang H, Yang D (2017) Embedding ultrafine and high-content Pt nanoparticles at ceria surface for enhanced thermal stability. Adv Sci 4(2017):1700056
11. Li S, Bao D, Shi M, Wu B-L, Yan J, Jiang Q (2017) Amorphizing of Au nanoparticles by CeO_x-RGO hybrid support towards highly efficient electrocatalyst for N_2 reduction under ambient conditions. Adv Mater 29:1700001
12. Jin R, Zeng C, Zhou M, Chen Y (2016) Atomically precise colloidal metal nanoclusters and nanoparticles: fundamentals and opportunities. Chem Rev 116:10346–10413

13. Zhan W, He Q, Liu X, Guo Y, Wang Y, Wang L, Guo Y, Borisevich A-Y, Zhang J, Lu G, Dai S (2016) A sacrificial coating strategy toward enhancement of metal–support interaction for ultrastable Au nanocatalysts. J Am Chem Soc 138:16130–16139
14. Mitsudome T, Mikami Y, Matoba M, Mizugaki T, Jitsukawa K, Kaneda K (2012) Design of a silver-cerium dioxide core–shell nanocomposite catalyst for chemoselective reduction reaction. Angew Chem Int Ed 51:136–139
15. Han YJ, Han L, Zhang LL, Dong SJ (2015) Ultrasonic synthesis of highly dispersed Au nanoparticles supported on Ti-based metal-organic frameworks for electrocatalytic oxidation of hydrazine. J Mater Chem A 3:14669–14674
16. Jiao Y, Li N, Yu H, Li W, Zhao J, Li X, Zhang X (2017) Fabrication of strawberry-like Au@CeO_2 nanoparticles with enhanced catalytic activity by assembly of block copolymer composite micelles. RSC Adv 7:662–668
17. Song S, Wang X, Zhang H (2015) CeO_2-encapsulated noble metal nanocatalysts: enhanced activity and stability for catalytic application. NPG Asia Material 7:179
18. Wang F, Wang J, Shao L, Zhao Y, Xia X (2014) Hybrids of gold nanoparticles highly dispersed on graphene for the oxygen reduction reaction. Electrochem Commun 38:82–85
19. Zhang C, Wang G, Ji Y, Liu M, Feng Y, Zhang Z (2010) Enhancement in analytical hydrazine based on gold nanoparticles deposited on ZnO-MWCNTs films. Sensors Actuators B Chem 150:247–253
20. Ismail RA, Abdul-Hamed R (2017) Laser ablation of Au–CuO core–shell nanocomposite in water for optoelectronic devices. Mater Res Express 4:125020
21. Ye W, Yang B, Cao G, Duan L, Wang C (2008) Electrocatalytic oxidation of hydrazine compound on electroplated Pd/WO_3 film. Thin Solid Films 516:2957–2961
22. Costa WM, Marques AB, Marques EP, Bezerra CB, Sousa ER, Cardoso WS, Song CJ, Zhang JJ (2010) Hydrazine oxidation catalyzed by ruthenium hexacyanoferrate-modified glassy carbon electrode. J Appl Electrochem 40:375–382
23. Zhao Z, Xia Z, Liu C, Huang H, Ye W (2017) Green synthesis of Pd/Fe_3O_4 composite based on polyDOPA functionalized reduced graphene oxide for electrochemical detection of nitrite in cured food. Electrochim Acta 256:146–154
24. Abdel-mageed A, Kucerova G, Bansmann J, Behm R (2017) Active Au species during the low-temperature water gas shift reaction on Au/CeO_2: a time-resolved operando XAS and DRIFTS study. ACS Catal 7:6471–6484
25. Wang H, Thia L, Li N, Ge X, Liu Z, Wang X (2015) Selective electro-oxidation of glycerol over Au supported on extended poly(4-vinylpyridine) functionalized graphene. Appl Catal B Environ 166:25–31
26. Bard A, Faulkner L (2001) Fundamentals and application in: electrochemical method. Wiley New York
27. Benvidi A, Jahanbani S, Mirjalili B, Zare R (2016) Electrocatalytic oxidation of hydrazine on magnetic bar carbon paste electrode modified with benzothiazole and iron oxide nanoparticles: simultaneous determination of hydrazine and phenol. Chin J Catal 37:549–560
28. Pournaghi-Azar M, Sabzi R (2003) Electrochemical characteristics of a cobalt pentacyanonitrosylferrate film on a modified glassy carbon electrode and its catalytic effect on the electrooxidation of hydrazine. J Electroanal Chem 543:115–125
29. Zhu Y, Sigdel A, Zhang S, Su D, Xi Z, Li Q, Sun H (2014) Angew Chem Int Edit 126:12716–12720
30. Hamidi H, Bozorgzadeh S, Haghighi B (2017) Amperometric hydrazine sensor using a glassy carbon electrode modified with gold nanoparticle-decorated multiwalled carbon nanotubes. Microchim Acta 184:4537–4543
31. Guo W, Ma J, Cao X, Tong X, Liu F, Liu Y, Liu S (2017) Amperometric sensing of hydrazine using a magnetic glassy carbon electrode modified with a ternary composite prepared from Prussian blue, Fe_3O_4 nanoparticles, and reduced graphene oxide. Microchim Acta 184:3163–3170
32. Yang Z, Sheng Q, Zhang S, Zheng X, Zheng J (2017) One-pot synthesis of Fe_3O_4/polypyrrole/graphene oxide nanocomposites for electrochemical sensing of hydrazine. Microchim Acta 184: 2219–2226
33. Rahman MM, Khan A, Marwani HM, Asiri AM (2016) Hydrazine sensor based on silver nanoparticle-decorated polyaniline tungstophosphate nanocomposite for use in environmental remediation. Microchim Acta 183:1787–1796
34. Rahman MM, Alam MM, Asiri AM (2018) Selective hydrazine sensor fabrication with facile low-dimensional Fe_2O_3/CeO_2 nanocubes. New J Chem 42:10263–10270